

Scaling Wake-Particle Interactions for Aerial Applications Research

Allen I. Ormsbee,* Michael B. Bragg,† and Mark D. Maughmer‡

University of Illinois, Urbana, Ill.

and

Frank L. Jordan§

NASA Langley Research Center, Hampton, Va.

The differential equation for the trajectory of a spherical particle injected into an aircraft wake was developed and the proper scaling relations extracted. After some simplification, a convenient set of similarity parameters was established. Using these similarity parameters a scale-model test program was designed and performed in the NASA Langley Vortex Research Facility. The results of the tests demonstrated the validity of the similarity parameters in conducting scale-model testing for aerial applications research.

Nomenclature

b	= wing span
C_D	= drag coefficient, D/qS
C_L	= lift coefficient, L/qS
d	= propeller diameter
g	= gravitational constant
h	= model height (wing tip)
m	= mass of particle
n	= propeller angular velocity
R	= Reynolds number
t	= time
u	= particle velocity
U	= freestream velocity (model speed)
V_r	= particle relative velocity
X	= particle position vector
Γ	= characteristic circulation for the wing
Γ_p	= characteristic circulation for the propeller
δ	= particle diameter
θ_p	= propeller angular position
μ	= absolute air viscosity
η	= nondimensional particle position
ρ	= air density
σ	= particle density
<i>Superscripts</i>	
(\cdot)	= derivative with respect to time
$(\cdot)'$	= derivative with respect to nondimensional time ($\tau = Ut/b$)
(\cdot)	= vector notation

Introduction

CURRENTLY the National Aeronautics and Space Administration is engaged in research directed toward advancing aerial applications technology. As reported in Ref.

Presented as Paper 80-1873 at the AIAA Aircraft Systems and Technology Meeting, Anaheim, Calif., Aug. 4-6, 1980; submitted Sept. 12, 1980; revision received Jan. 5, 1981. Copyright © American Institute of Aeronautics and Astronautics, Inc., 1980. All rights reserved.

*Professor, Department of Aeronautical and Astronautical Engineering. Associate Fellow AIAA.

†Research Associate (currently Graduate Research Associate, Ohio State University). Member AIAA.

‡Graduate Research Assistant. Member AIAA.

§Aerospace Technologist. Member AIAA.

1, one aspect of the program is aimed at a better understanding of the interaction of the dispersed substance with the aircraft wake. The ultimate goal is the capability to modify the aircraft wake characteristics and integrate with it the dispersal system in such a way as to obtain a wide, uniform distribution of the material on the ground with a minimum of the material being lost due to drift. Although some full-scale agricultural aircraft deposition data have been obtained, the large number of variables which are difficult to control and measure in a flight test of this type make these data of limited value. On the other hand, small-scale model tests would provide strictly controlled conditions where research may be conducted and data generated more efficiently and accurately, provided that the results could be extrapolated correctly to the full scale. The development of the capability to simulate full-scale wake-particle interaction should provide a highly efficient research tool to generate baseline data which are not currently available, as well as to provide a means by which advanced aircraft configurations and dispersal concepts may be evaluated.

The goal of this research effort was twofold: 1) to develop from theory the appropriate similarity parameters for wake-particle interaction, and 2) to verify these similarity parameters experimentally using a small-scale model test. The first part of this effort relied heavily upon Refs. 2 and 3 in its initial stages. The results of the similarity analysis have been reported in detail by Ormsbee and Bragg.⁴ The important results from this paper will be presented in the next section.

The second part of this study has been presented in detail in Ref. 5. Before the verification of the scaling laws could be attempted the experimental techniques for testing small-scale agricultural aircraft had to be developed. The tests were conducted in the NASA Langley Vortex Research Facility, and many of the experimental procedures pertain only to this facility. This paper will describe only that part of the experimental technique necessary to substantiate the data and results. For a more detailed description, see Refs. 1 and 5. It is important to note the experimental data presented were generated to test the applicability of the similarity analysis, and should not be misconstrued as baseline data for some agricultural aircraft.

Theoretical Development

Physical Model

In this section similarity parameters are developed to allow small-scale model testing of aircraft aerial application systems. The approach is to develop a model for the physical

process and derive for this model the appropriate governing equations. From the nondimensional forms of the governing equations the scaling parameters are extracted. By rearranging these parameters and further simplifying them, the set of scaling parameters needed to conduct small-scale model tests are derived.

To expedite the analysis of this system many simplifications are made in the development of this model. First, it is assumed that the number of particles is sufficiently small that particle-particle interaction may be ignored. This assumption, allowing the study of a single-particle trajectory, is consistent with current spraying practice. Another simplification is made by assuming that the particles are spherical, allowing the use of standard sphere drag curve fits. For liquids, particles (droplets) in the 100-500 μm size range are nearly spherical in shape.⁶ In addition the effect on the particle trajectory of atmospheric- and aircraft-induced turbulence, liquid droplet deformation and internal circulation, magnus forces, droplet evaporation, and electric charge is considered negligible. The model does allow dry materials of larger than 100 μm , provided they are spherical.

The equation of motion for a single particle moving in an aircraft wake can be written in vector form as^{7,8}

$$\ddot{M}\ddot{X} = \bar{D} + \bar{P} + \bar{M}_a + \bar{B} + Mg \quad (1)$$

in an aircraft-fixed coordinate system where the flow is steady. \bar{P} , \bar{M}_a , and \bar{B} represent the pressure gradient, the apparent mass, and the Bassett force, respectively. The densities of typical particles are much greater than that of air; therefore, the apparent mass term is neglected.⁷ For a particle in the potential region of the wake, no significant pressure gradient exists and the pressure gradient term may be neglected. The numerical program of Ref. 3 was used to determine that a particle will experience a large acceleration only when first injected into the flowfield, and that this acceleration is of short duration. Bassett forces are significant only for large particle accelerations; therefore, this term is neglected.

With only the drag and gravity terms remaining on the right-hand side, Eq. (1) becomes

$$\ddot{X} = \frac{\rho C_D}{\delta\sigma} |\ddot{u} - \dot{\bar{X}}| (\ddot{u} - \dot{\bar{X}}) + g \quad (2)$$

The wake of an aircraft can be characterized by relatively confined regions of vorticity bounded by regions of irrotational flow. By confining the particle to only the region of irrotational flow, the velocity field \ddot{u} may be modeled using potential flow concepts. Although the detailed accuracy of such a wake model may be questioned, the intent here is not an accurate wake flowfield model. The model need only contain the important variables in the correct relationships. The expression for the flowfield velocity is then written in functional form as

$$\ddot{u} = \frac{\Gamma}{b} \bar{F} \left(\frac{\dot{X}}{b}, \frac{h}{b}, \frac{\Gamma}{\Gamma_p}, \frac{U}{nd}, \frac{d}{b}, \theta_p \right) + \bar{U} \quad (3)$$

Sphere drag data have been obtained by many researchers and a standard sphere drag curve has been established for a nonaccelerating sphere.⁹ Several researchers have developed curve fits to these data which are of the form

$$C_D = \sum_{i=0}^N C_i R^{\alpha_i} \quad (4)$$

The particle Reynolds number R is given by

$$R = \rho\delta V_r U / \mu, \quad V_r = |\ddot{u} - \dot{\bar{X}}| / U$$

Similarity Analysis

Substituting Eqs. (3) and (4) into Eq. (2) yields, after some manipulation,

$$\frac{U^2}{bg} \ddot{\eta}'' = \frac{1}{4} \sum_{i=0}^N \left(\frac{C_i \rho^{1+\alpha_i} \delta^{\alpha_i-1} U^{2+\alpha_i} V_r^{1+\alpha_i}}{\sigma g \mu^{\alpha_i}} \bar{V}_r \right) + \frac{\bar{g}}{g} \quad (5)$$

Inserting

$$\bar{V}_r = \Gamma \bar{F} / Ub + \bar{U} / U - \bar{\eta}'$$

into Eqs. (3) and (5), the equation of the particle trajectory can be expressed in functional form,

$$\ddot{\eta} = G \left(\frac{U^2}{bg}, \frac{\Gamma}{Ub}, \frac{Ut}{b}, \frac{h}{b}, \frac{\Gamma}{\Gamma_p}, \frac{U}{nd}, \frac{d}{b}, \theta_p, \frac{\rho\delta U}{\mu}, \frac{\rho^2 U^3}{\sigma g \mu} \right) \quad (6)$$

where the N nondimensional parameters from Eq. (5) reduce to the last two terms in Eq. (6).

The terms on the right-hand side of Eq. (6), when held constant between two geometrically similar models, will assure identical nondimensional particle trajectories, providing the nondimensional initial conditions on the particle are the same. Before the discussion of all of the similarity parameters, note that the particle diameter and density appear only in the last two terms. Here ρ , μ , and g are considered fixed since for most model tests they cannot be controlled. This leads to the particle diameter and density as a function of U only, where U is given for a certain scale model by the first term. Equation (6) for a small-scale model test requires that a unique particle must be used which is much larger in diameter and has a density much less than that of the full-scale particle being simulated. This leads to two problems, one practical and one in the theoretical model. Practically, such large-diameter, low-density spheres are difficult to obtain and Eq. (6) provides no alternative solutions. For very small-scale models the particle density required may be so low as to violate the assumptions made in the derivation of Eq. (2), therefore making invalid the entire scaling argument. The pressure gradient and apparent mass terms cannot be neglected if the particle density is of the same order as that of air.

To avoid the problems created by a unique low-density scaled particle, a further assumption is made. Assume that for the range of particle Reynolds numbers seen by the full-scale and the appropriate scaled particle, Eq. (4) may be approximated by only one term, $C_D = CR^\alpha$. Substituting this into Eq. (5), Eq. (6) becomes

$$\ddot{\eta} = H \left(\frac{U^2}{bg}, \frac{\Gamma}{Ub}, \frac{Ut}{b}, \frac{h}{b}, \frac{\Gamma}{\Gamma_p}, \frac{U}{nd}, \frac{d}{b}, \theta_p, \frac{\rho^{1+\alpha_0\alpha-1} U^{2+\alpha}}{\sigma g \mu^\alpha} \right) \quad (7)$$

Using the computer program of Ref. 3 it has been found that, after their initial deceleration when injected into the wake, particles experience Reynolds numbers only slightly larger than their terminal Reynolds numbers. Using this information, an iterative approach is used to determine C and α in the drag coefficient equation.

The nondimensional terms in Eq. (7) are the scaling parameters needed to scale the trajectory of a single particle in an aircraft wake, with the same nondimensional initial conditions, between two geometrically similar models. The first eight parameters scale the aircraft flowfield. The first term in Eq. (7) is the square of the Froude number. This parameter determines the model test velocity. The second parameter is the nondimensional vortex strength. Since the

aircraft operates at moderate lift coefficients and at low Mach numbers, it is reasonable to assume Reynolds number and Mach number independence of the flowfield; therefore, the second parameter requires operation at a fixed angle of attack. Nondimensional time is given by the third term, and the fourth term requires that the nondimensional height of the aircraft above the ground plane be held constant. The fifth through eighth terms deal with the scaling of the propeller slipstream. Parameters to be held constant are, respectively, the ratio of wing to propeller vortex strength, the advance ratio, the geometrical scale of the propeller diameter, and the angular orientation of the propeller when the particle is injected into the flow. The last parameter of Eq. (7), as discussed previously, fixes the scaled particle diameter and density. As a result of the simple drag law assumed, an infinite number of candidate scaled particles now exist. This provides the experimentalist more freedom in the selection of test particles, and also enables the particle density to remain sufficiently large to insure the validity of Eq. (2) for very small-scale models.

Experimental Results

Experimental Techniques

The experimental data were obtained in the Langley Vortex Research Facility, shown in Fig. 1, in which a test model was moved through stationary air, a desirable feature in the study of ground deposition patterns behind an agricultural aircraft. The model is strut mounted below a vehicle which travels on an overhead track and propels the model through an enclosed test section with a ground plane. Additional details concerning this facility can be found in Refs. 1 and 5.

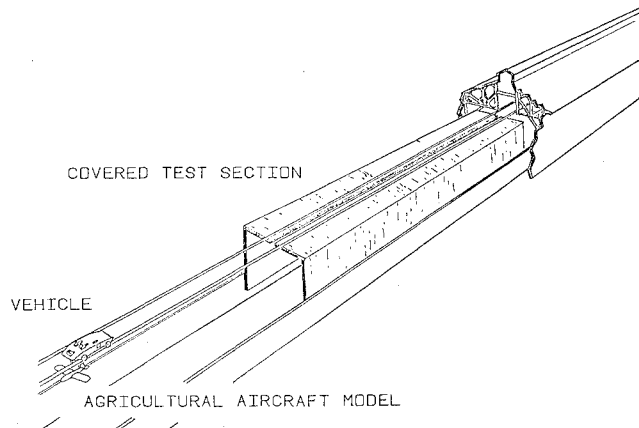


Fig. 1 NASA Langley Vortex Research Facility.

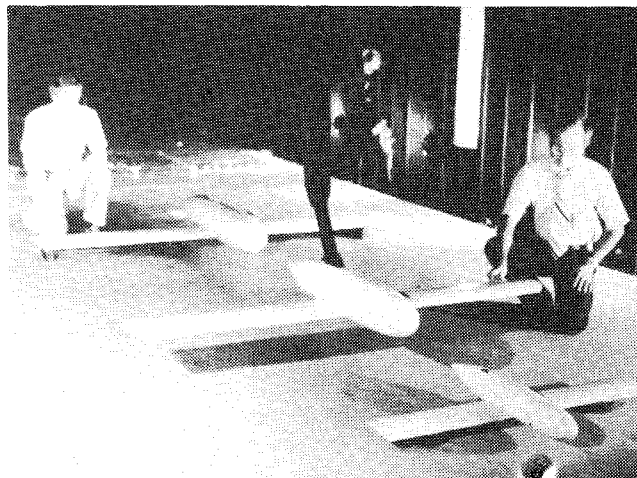


Fig. 2 Unpowered models shown in the Vortex Research Facility.

Because meaningful full-scale data were unavailable, the experimental program to validate the scaling laws had to be self-contained. Three geometrically similar wing-fuselage models were used to examine the single-ejector ground depositions with test conditions and particle characteristics dictated by the scaling laws. The three models, shown in Fig. 2, with spans of 1.22, 1.83, and 2.44 m (4.6, and 8 ft), were designed to be 0.10, 0.15, and 0.20 scale models of a hypothetical full-scale aircraft having a span of 12.2 m (40 ft) and a flight speed of 53.3 m/s (119 mph). Tests were conducted with and without operational scaled propellers. Powered effects were based on a full-scale powerplant of 300 kW (401 hp) operating a 2.49 m (8.2 ft) diam propeller at 2308 rpm with an 85% propeller efficiency. As required by the scaling laws, the thrust coefficient C_T of 0.068 and the advance ratio J of 0.56 were held constant. The model propellers were driven by a pneumatic motor.

The particles were placed in containers inside the wings and allowed to gravity feed out of ejectors under the wing. At a specified location on the test section ground plane, the particles were collected on adhesive strips for data reduction. The data were reduced in terms of particles per square semispan, a unit of concentration. No attempt was made to scale nozzle characteristics or a specific dispersal system as our purpose was only to validate the similarity parameters and not to generate meaningful baseline data.

Application of Scaling Parameters

A baseline configuration was chosen for the hypothetical full-scale aircraft and scaled to each of the models. About this baseline, variation in C_L , h , particle size, and power effects were studied as they related to the scaling validation. Table 1 indicates the scaled physical variables obtained from the application of Eq. (7). After an extensive search of commercially available spherical particles, glass microbeads which scaled as close to a common full-scale water droplet as possible were chosen for the baseline. These particles were sized within $\pm 10\%$ of the median diameter and $\pm 5\%$ of the median density. Although the intent was to scale a single particle, this distribution does roughly scale among the models. The 0.10 and 0.15 scale models were also tested using fillite spheres which scaled to a 200 μm , full-scale water droplet.

Although only two scale models would have been necessary, the 2.44 m span model was built as it was felt that such a large model, spanning approximately one-half the test section width, would be useful in evaluating a test envelope for the facility. A test envelope was generated theoretically and verified experimentally for the facility.⁵ Only the two smaller models were used for the off-baseline tests to insure that all data were taken within the facility test envelope and to reduce the number of tests needed.

Results and Discussion

Figure 3 shows measured ground deposition patterns comparing the three baseline models with ejectors at the 0.2 and 0.6 semispan stations. From these data were calculated the median which is used on the summary plots.

Table 1 Baseline physical variables

	Model scale			
	0.10	0.15	0.20	1.0
b, m	1.22	1.83	2.44	40.0
d, m	0.249	0.373	.498	2.49
h, m	0.622	0.933	1.24	20.4
n, rpm	7300	5970	5170	2310
$U, \text{m/s}$	16.8	20.6	23.8	53.3
α, deg	2.00	2.00	2.00	2.00
$\delta, \mu\text{m}$	105.0	125.0	105.0	490.0
$\sigma, \text{g/cm}^3$	2.42	2.42	3.99	1.0

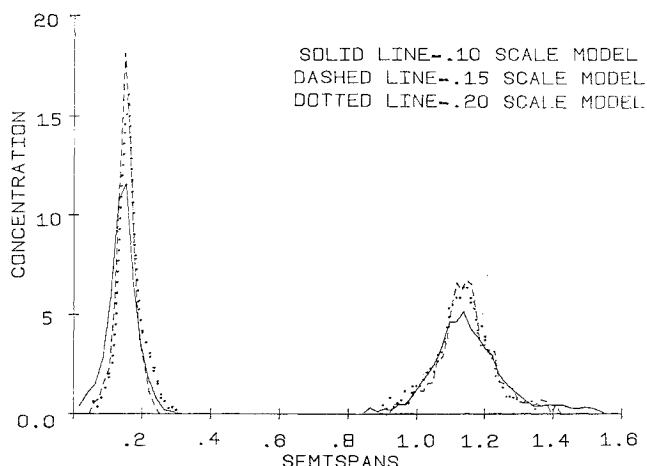


Fig. 3 Baseline ground depositions from ejectors at 0.2 and 0.6 semispans.

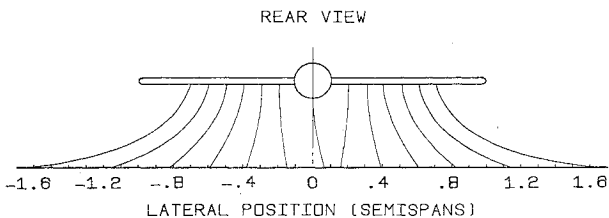


Fig. 4 Median deposition trajectories for the propeller-off baseline ($H = 0.51$ semispans, $C_L = 0.61$, particle size = $490 \mu\text{m}$).

During data reduction, errors were more likely to occur at the edges of the distributions where the particles were difficult to distinguish from the noise in the system. Consequently, the median was used since these errors have less effect on the median of the ground distributions than on the mean. Note in Fig. 3 that as the particle ejector is moved toward the wing tip, the increased lateral transport of the particles due to the wing-tip vortices causes a reduction in the maximum concentration and an increase in the width of the distribution. The finite width of the concentration patterns is due primarily to the variations in particle diameter and density about the median particle. The concentration patterns compare quite well among the models. This indicates that with more careful attention given to the scaling of an entire particle distribution, future tests should be able to scale actual particle diameter and density distributions.

Figure 4 pictorially represents a rear view of the model in which the particle trajectory and the median ground deposition location from each of the ejectors are depicted for the propeller-off baseline configuration. For example, a particle ejected at 0.6 semispans is transported by the vortex system to 1.13 semispans where it lands on the ground plane. The effect of the wing-fuselage intersection vortex is seen on particles ejected inboard of the 0.25 semispan station. It would be expected that at the centerline the left and right vortex systems would cancel, causing the particles here to fall straight downward. Two explanations for this possible discrepancy are given: first, only a limited amount of data were collected here, using only the 0.15 scale model; and second, this region is extremely sensitive to yaw angle or other model misalignment.

Figures 5-7 are summary plots of the lateral displacement of the median plotted against the ejector position. The lateral displacement of the median is the median ground deposition point minus the corresponding initial ejector location spanwise. Therefore for the baseline case, the solid line, at an ejector location of 0.4 semispans the lateral displacement is

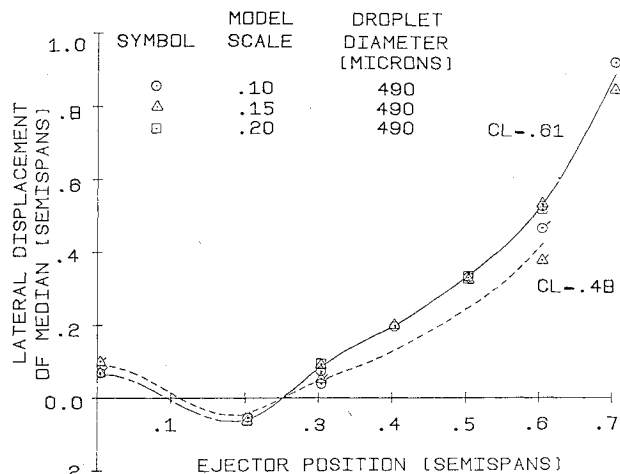


Fig. 5 Lateral displacement of deposition median as a function of ejector positions for varying lift coefficients ($H = 0.51$ semispans, particle size = $490 \mu\text{m}$).

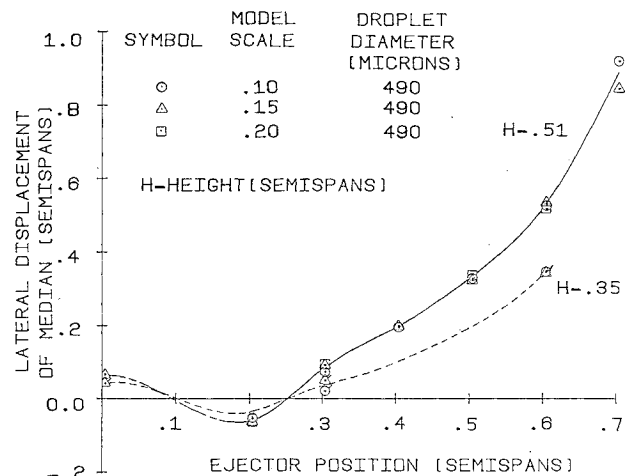


Fig. 6 Lateral displacement of deposition median as a function of ejector position for varying model heights ($C_L = 0.61$, particle size = $490 \mu\text{m}$).

about 0.2 semispans, meaning that the median ground deposition location was at 0.6 semispans. Figures 5-7 all indicate the baseline as a solid line with a dashed line for the part of the curve between 0.2 and 0 semispans due to the uncertainty in the data point at the centerline. The agreement among the three models is excellent and indicates the validity of the scaling analysis.

To reinforce the scaling verification, perturbations were made from the baseline in model lift coefficient, model height above the ground plane, and scaled particle size. Figure 5 indicates the effect of reduced model lift coefficient. Data were taken using only the 0.10 and 0.15 scale models to reduce the number of runs and to insure that the tests were within the facility test envelope. The result is to reduce the lateral transport of the particles and again the data compare well between the two scale models, providing further verification of the scaling analysis. Figure 6 shows the effect of model height on the lateral transport. The effect is similar to that of lowering the lift coefficient: the lateral transport of the particles is reduced.

The effect of varying model scale and droplet diameter is shown in Fig. 7. In order to examine the sensitivity of the deposition to these parameters, experiments were run in which the particles used did not scale to a common full-scale droplet. The importance of properly scaling experimental particles can be realized by the significant shifts that occur in the

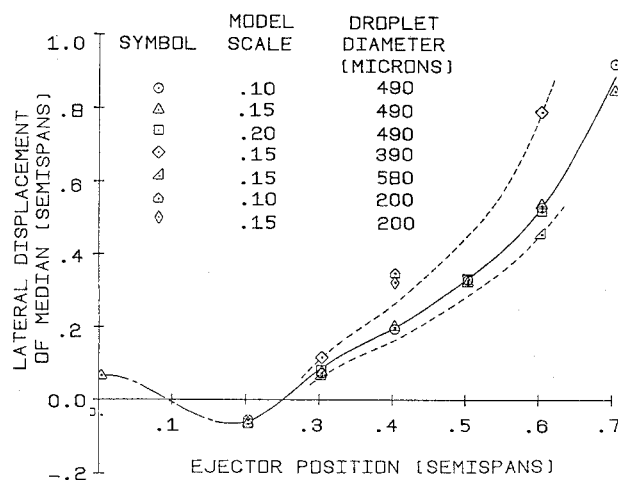


Fig. 7 Lateral displacement of deposition median as a function of ejector position for varying particle size ($C_L = 0.61$, $H = 0.51$ semispans; $H = 0.35$ semispans for case of particle size = 200 μm).

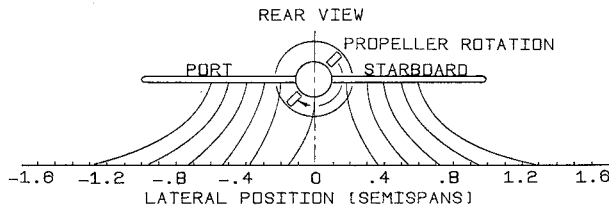


Fig. 8 Median deposition trajectories for propeller-on baseline scaling law validation experiments ($H = 0.51$ semispans, $C_L = 0.75$, particle size = 490 μm).

deposition medians when 390 or 580 μm scaled particles are used. In order to assure that the scaling validation was not coincidental to the 490 μm , full-scale droplet, an independent validation was performed by ejecting scaled 200 μm droplets from the 0.4 ejector position for the 0.10 and the 0.15 scale models. These tests were performed at $h = 0.35$ semispans and the results are shown in Fig. 7. This comparison again shows excellent agreement.

The results of propeller-on baseline tests are reported in Figs. 8 and 9. It must be emphasized that only a minimum number of runs were made in obtaining the propeller-on data. Therefore, these data must be considered as preliminary and final judgment on the propeller scaling must await further study. Some qualitative comments may, however, be made.

Figure 8 summarizes the data pictorially. The particles injected from inboard locations are displaced to the left due to the propeller slipstream. The propeller has little effect on the particles injected out of the slipstream as shown by the trajectories initiating from the ± 0.30 and the ± 0.60 semispan locations. Figure 9 shows the preliminary scaling validation for the propeller-on case and the baseline propeller-off case (solid line) for comparison. For the left side (dotted line), the scales indicate negative values to aid in the comparison. Outside of the 0.30 semispan location the left and right sides appear unaffected by the propeller, except for an upward shift in the graph. It is felt that this is due to an increase in lift coefficient due to the slipstream effect for the propeller-on case since the model was kept at a constant angle of attack of 2 deg. Inside the 0.3 semispan location the slipstream has a large effect as seen in Fig. 8. Although the propeller-on scaling results do not compare as well as the propeller-off case, the data are preliminary and show

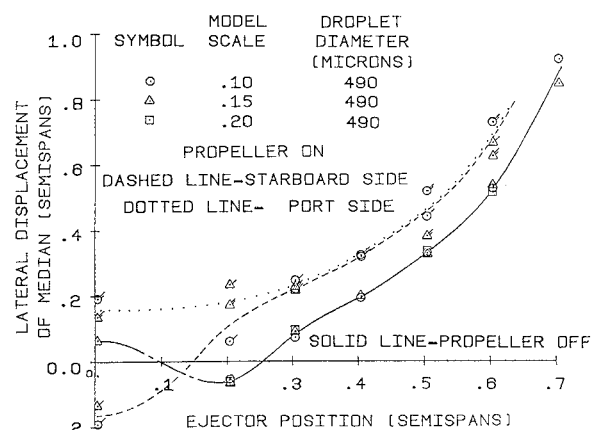


Fig. 9 Lateral displacement of deposition median as a function of ejector position for the baseline scaling law validation experiments ($H = 0.51$ semispans, $C_L = 0.75$; propeller-on case, particle size = 490 μm).

reasonable agreement. Propeller-on tests are significantly more difficult to conduct and control. More data are needed before any firm conclusions can be drawn concerning the propeller scaling.

Conclusions

Based on the experimental results of this research program, it is clear that the scaling laws developed provide a proper scaling of the particle dynamics and the flowfield as is necessary for the small-scale modeling of agricultural aircraft. The use of this similarity analysis to establish the test parameters for experiments covering a wide range of conditions provided significant agreement between the results of commonly scaled tests. The ability to scale wake-particle interaction and conduct small-scale model tests should prove to be a valuable research tool.

Acknowledgment

The study was supported by NASA Langley Research Center under Grant NSG 1434.

References

- 1 Jordan, F.L., McLemore, H.C., and Bragg, M.B., "Status of Aerial Applications Research in the Langley Vortex Research Facility and the Langley Full Scale Wind Tunnel," NASA TM 78760, Aug. 1978.
- 2 Reed, W.H., "An Analytical Study of the Effects of Airplane Wake on the Lateral Dispersion of Aerial Sprays," NACA Rept. 1196, 1954.
- 3 Bragg, M.B., "The Trajectory of a Liquid Droplet Injected Into the Wake of an Aircraft in Ground Effect," Aeronautical and Astronautical Engineering Dept., University of Illinois, Technical Rept. 77-7, UIUC-ENG 770507, May 1977.
- 4 Ormsbee, A.I. and Bragg, M.B., "Trajectory Scaling Laws for a Particle Injected Into the Wake of an Aircraft," Aviation Research Laboratory, Institute of Aviation, University of Illinois, Rept. ARL-78-1, June 1978.
- 5 Ormsbee, A.I., Bragg, M.B., and Maughmer, M.D., "The Development of Methods for Predicting and Measuring Distribution Patterns of Aerial Sprays," Aviation Research Laboratory, Institute of Aviation, University of Illinois, Rept. ARL-79-1, June 1979.
- 6 Hughes, R.R. and Gilliland, E.R., "The Mechanics of Drops," *Chemical Engineering Progress*, Vol. 48, No. 10, 1952, pp. 497-504.
- 7 Soo, S.L., *Fluid Dynamics of Multiphase Systems*, Blaisdell Publishing Co., Waltham, Mass., 1967.
- 8 Rudinger, G., "Flow of Solid Particles in Gases," AGARDograph 222, 1976, pp. 55-86.
- 9 Schlichting, H., *Boundary Layer Theory*, 6th ed., McGraw-Hill Book Co., New York, 1968.